Available online at www.sciencedirect.com

ScienceDirect
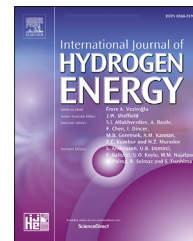
Magnetic field enhancement of electrochemical hydrogen evolution reaction probed by magneto-optics

Olga Sambalova [a,b], Emanuel Billeter [a,b], Oguz Yildirim [c], Andrea Sterzi [a], Davide Bleiner [a], Andreas Borgschulte [a,b,]*

[a] *Laboratory for Advanced Analytical Technologies, Empa - Swiss Federal Laboratories for Material Science and Technology, Überlandstrasse 129, 8600, Dübendorf, Switzerland*
[b] *Department of Chemistry, University of Zurich, Winterthurerstrasse 190, 8057, Zürich, Switzerland*
[c] *Laboratory for Magnetic and Functional Thin Films, Empa - Swiss Federal Laboratories for Material Science and Technology, Überlandstrasse 129, 8600, Dübendorf, Switzerland*

HIGHLIGHTS

- Magnetic field effects on hydrogen evolution probed by in situ magneto-optics.
- External magnetic fields enhance electrochemical hydrogen evolution on Pt.
- The effect is linked to the magnetic changes of the electrochemical double layer.

ARTICLE INFO

ABSTRACT

External magnetic fields affect various electrochemical processes and can be used to enhance the efficiency of the electrochemical water splitting reaction. However, the driving forces behind this effect are poorly understood due to the analytical challenges of the available interface-sensitive techniques. Here, we present a set-up based on magneto- and electro-optical probing, which allows to juxtapose the magnetic properties of the electrode with the electrochemical current densities in situ at various applied potentials and magnetic fields. On the example of an archetypal hydrogen evolution catalyst, Pt (in a form of Co/Pt superlattice), we provide evidence that a magnetic field acts on the electrochemical double layer affecting the local concentration gradient of hydroxide ions, which simultaneously affects the magneto-optical and magnetocurrent response.

* Corresponding author. Laboratory for Advanced Analytical Technologies, Empa - Swiss Federal Laboratories for Material Science and Technology, Überlandstrasse 129, 8600, Dübendorf, Switzerland.
E-mail address: andreas.borgschulte@empa.ch (A. Borgschulte).

Introduction

Water electrolysis is widely recognized as one of the key processes for accelerating the use of renewable energy [1—5]. For decades there has been a growing effort to increase the efficiency of the process. However, state-of-the-art alkaline and polymer electrolyte membrane electrolyzer efficiencies (70% and 82%, respectively [6—9]) are only slightly higher than 100 years ago [10]. Surprisingly, recently a drastically increased electrochemical efficiency was achieved simply by applying a uniform magnetic field to the oxygen evolution electrode [11]. Electrochemical magnetic enhancement was observed also for hydrogen evolution reaction of different systems [12,13]. Currently there is no consensus about the driving force that justifies the observations. The effect is particularly unexpected, as typical magnetic energies are orders of magnitude lower than chemical energies (energy of spin-spin interactions $< \mu J \ mol^{-1}$) [14] and the expected contribution of the magnetic field to increasing the rate of chemical reactions is effectively zero from a purely thermodynamic perspective.

Most of the known effects of magnetic fields on electrochemical processes are magneto-hydrodynamic in nature and stem from the Lorentz force. External magnetic fields potentially influence: 1) the capacitance, resistance and "thickness" of the electrochemical double layer [15], 2) surface morphology of the electrode [16], 3) diffusion layer kinetics [17,18], 4) formation, size and stability of surface bubbles [19], and 5) reaction kinetics, especially when radical species are involved [14,20,21].

Despite the many available analytical techniques for probing electrochemical reactions, their in situ analysis remains a challenge. Particular difficulty lies in retaining surface sensitivity in the presence of the bulk electrolyte, while maintaining the often extreme pH environment and ambient or elevated temperature and pressure. For example, photoelectron spectroscopies are strongly surface sensitive, but are mostly restricted to ultra high vacuum conditions. One of the techniques that offers non-destructive analysis that is compatible with the outlined requirements is based on magneto-optics [22]. Briefly, magneto-optical probing is based on the difference between the refractive indices of the right and left circularly polarized components of linearly polarized incident electromagnetic radiation. This difference develops as light passes through (Faraday effect) or is reflected by (Kerr magneto-optical effect) a birefringent medium exposed to a magnetic field. In case of electrochemical probing, additional contribution (Pockels effect) arises from non-centrosymmetric components exposed to an electric field. The surface sensitivity of around 5 nm is estimated by the attenuation of light in metals. Although it is designed to probe magnetic properties, non-magnetic or weakly magnetic materials can be analyzed indirectly. For example, Pt can be used as an active interface to the electrolyte in a form of a Co/Pt supperlattice, which is known for its strong perpendicular magnetic anisotropy and finite remanent magnetization [23].

In this work, we present an in situ approach that allows probing the electrode-electrolyte interface in an applied magnetic field, while simultaneously monitoring the magnetocurrent response (Fig. 1, for details refer to A) and summarize the assumptions. The magneto-optical response of Co/Pt multilayer with Pt layer (for further details refer to B) as the hydrogen evolution electrode yields information on structural and chemical changes of the electrode-electrolyte interface. We report a magnetic field induced change of over 7% percent in the electrochemical current density under constant applied bias of −0.15 V (vs RHE) and correlate this change to the magneto-optic response. In the discussion section, we provide evidence that this change is induced by the magnetic field gradient at the surface and provide possible explanations regarding the effect of the magnetic field on the electrolyte and on the electrode. Finally, we conclude that an applied external magnetic field strongly influences the current density of the hydrogen evolution reaction and the chemical composition of the electrochemical double layer.

Results

When light is reflected at a magnetic interface, the intensity and polarization of the transmitted/reflected light is modified by the layers interacting with the electromagnetic wave. For the chosen measurement principle, the following considerations were taken into account:

(i) The light absorption through the dielectric is assumed to be negligible. However, the Faraday effect of the electrolyte layer (3 mm optical path; aq. KOH) and the optical window (SiO_2) of the electrochemical cell is strong. The deconvolution of the Faraday contributors is not straightforward, as the effect is larger than the sought one (Fig. 1). Therefore, instead of evaluating the full response, we restrict the discussion to the difference signal between the two branches of the hysteresis curve $\Delta M \propto (\theta(B_{increasing}) - \theta(B_{decreasing}) = \oint \Delta M_B dB$, effectively removing all Faraday contributions. ΔM is directly related to the intrinsic magnetic properties of the Co/Pt thin film and is very sensitive to its morphology and chemical composition [24,25].

(ii) The orientational disorder of water in the EDL modifies its optical properties. The effective dipole moment of dynamically disordered bulk water is zero. As the molecules align at the interface, the effective dipole moment increases and becomes sensitive to an applied electric field [26]. This so-called Pockels effect depends on the refractive index n_{EDL} and scales linearly with the effective electric field at the interface.

(iii) During electrolysis the number of OH^- ions in alkaline electrolytes increases at expense of the water molecules at the hydrogen electrode surface, and vice versa at the oxygen electrode. In a very simplified way:
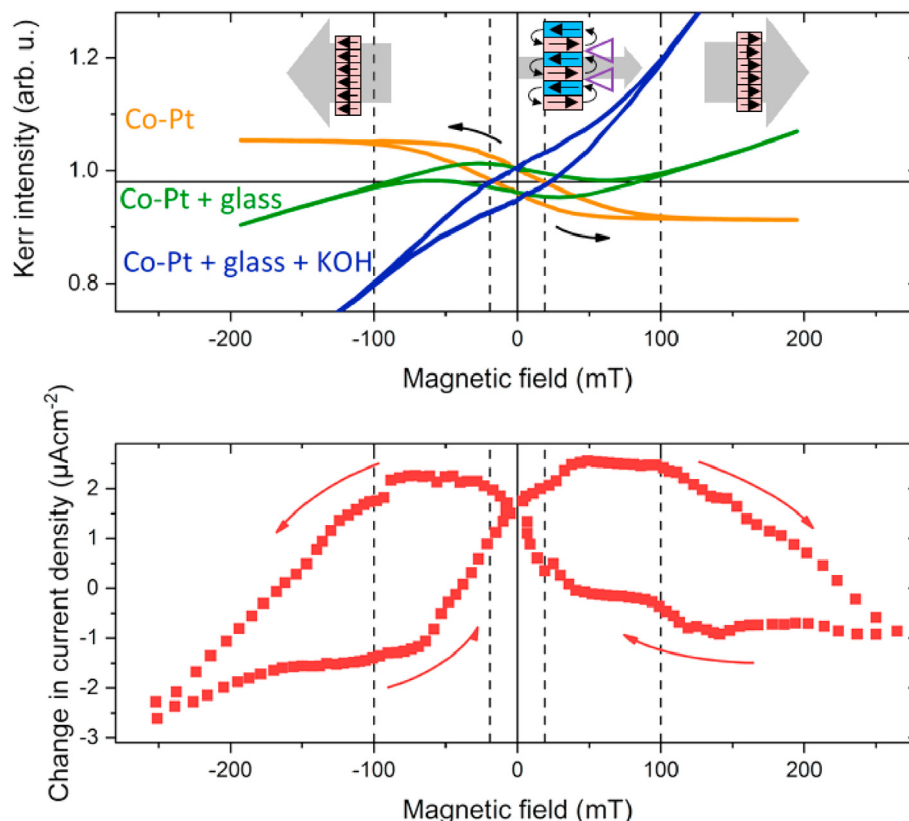 · hydrogen evolution reaction (cathode):

Fig. 1 – Top panel: MOKE hysteresis curves of Co/Pt in air (orange), with a glass optical window (green) and in 0.1 M KOH (blue). The sketches depict the magnetic domain structure causing magnetic stray fields and thus large local gradients near the interface at low applied magnetic fields. The dashed lines are drawn at the MOKE coercive fields and saturation points. Bottom panel: Magnetocurrent density measured in 0.1 M KOH at −0.15 V and 3 s per measurement point. (For interpretation of the references to colour in this figure legend, the reader is referred to the Web version of this article.)
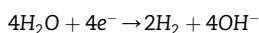
$$4H_2O + 4e^- \rightarrow 2H_2 + 4OH^- \tag{1}$$

· oxygen evolution reaction (anode):
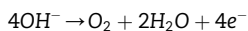
$$4OH^- \rightarrow O_2 + 2H_2O + 4e^- \tag{2}$$

The change in the ionic concentration affects the refractive index near the electrode. Unlike the Pockels effect, which scales with the electric field, ionic concentration is dependent on current density and time.

(iv) Overall, the magneto-optical response is affected by all the components of the electrochemical system: the optical window (Faraday), bulk electrolyte (Faraday), electrochemical double layer and diffusion layer (Faraday and Pockels effects) and the electrode (magneto-optical Kerr effect). In addition, the magneto-optical signal depends on the change in the refractive index, e.g. between a magneto-optical medium and a dielectric, here the EDL. The effect of the refractive index on the MOKE signal in a multilayered system has been defined previously [27]. Applying the same

relationship between the MOKE enhancement factor, f_e^c, and the MOKE rotation, θ, we get:

$$f_e^c = \frac{\theta(\widetilde{n}_{EDL}, \widetilde{n}_{CoPt})}{\theta(n_0, \widetilde{n}_{CoPt})} \tag{3}$$

where $\widetilde{n}_{CoPt} = const$ and $\widetilde{n}_{EDL} = f(U,B)$ are the complex refractive indices of the magnetically stable electrode and electrochemical double layer in a magnetic field, respectively, and $n_0 = 1$ is the refractive index of air, i.e. system in the absence of an electcrolyte (see section C for further details). The experimental enhancement, f_e, is defined as a change to the initial state, rather than an absolute value, i.e. $f_e \propto f_e^c$. The calculation estimates f_e^c values slightly less than unity, decreasing with increasing n_{EDL} for the given system (section C).

The power of the optical magneto-electrochemical set-up, as described in detail in A, lies in the simultaneous probing of the magneto-optics and magnetocurrents. Notably, in magneto-optic response, there is a progressive increase to the hysteresis area, ΔM, upon application of positive bias (oxygen evolution) and decrease upon application of negative bias (hydrogen evolution) (Fig. 2). However, no difference is observed in the shape of the hysteresis (Fig. S1), only the overall area. This signifies unchanged magnetic properties of the electrode during either hydrogen or oxygen evolution and
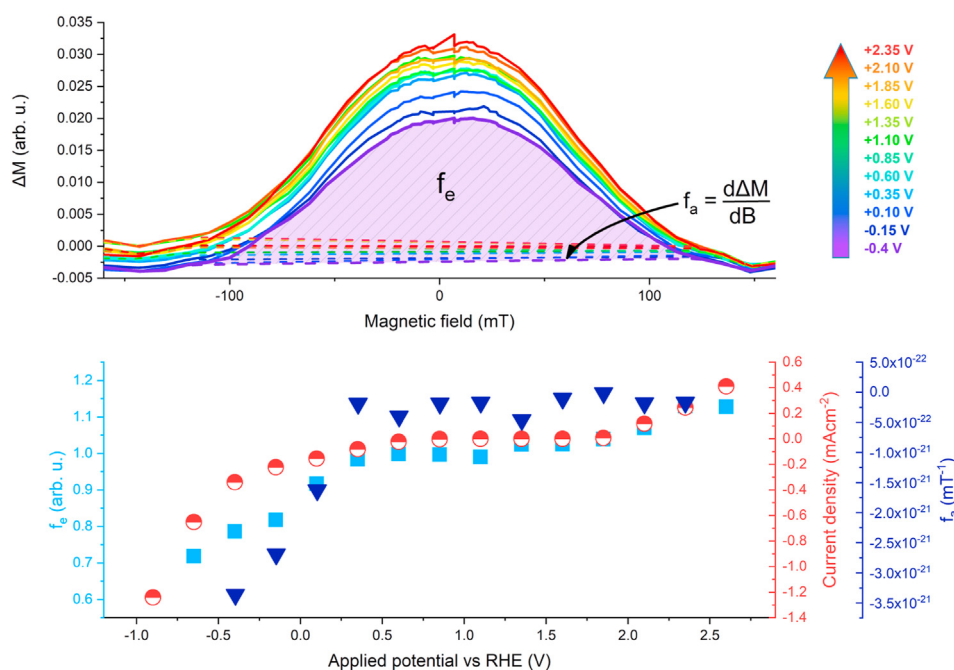
Fig. 2 — Top panel: the difference between two hysteresis branches ΔM at various applied potentials. The integrated area as indicated by the shading is used as relative Kerr enhancement factor f_e. The hysteresis area is not symmetric, from which the asymmetry factor f_a is derived. Bottom panel: Kerr enhancement, asymmetry factor, and current density as a function of the applied potential.

overall stability of the electrode under the given conditions, which is further confirmed by the pre- and post-catalytic XPS analysis (Fig. S2). This is not surprising, considering the electrochemical stability of the Pt layer that is in contact with the electrolyte. Therefore, the changes of the magneto-optical signal are not connected to the electrode ($\tilde{n}_{CoPt} = const.$), optical window ($\tilde{n}_{glass} = 1.52 = const.$) or bulk electrolyte ($\tilde{n}_{KOH} = 1.37 = const$ for 0.1 M KOH). On another hand, the refractive index of the interfacial electrolyte layers changes as a result of electrochemical processes (Eq. (1); $\tilde{n}_{EDL} = 1.37 + \Delta\tilde{n}$).

The bias-induced changes to the area of the hysteresis, ΔM, are directly proportional to the MOKE enhancement parameter f_e. The latter does not scale linearly with the applied bias, as would be the case with Pockels effect, but rather scales with the electrochemical current density (Fig. 2), in line with the assignment of the observed effect to the change in the refractive index near to the interface. This effect could originate from a change in the ion concentration or the thickness of the layer, according to equation C.1. Due to the non-linear scaling with the electric field, a contribution from the Pockels effect is assumed to be minor, even though it cannot be fully excluded.

Interestingly, there is a clear dependence on the magnetic field direction, which is particularly visible in the asymmetry of the MOKE signal between the high positive (>100 mT) and high negative (<−100 mT) magnetic fields (Fig. 2), defined by the assymetry factor, $f_a = \frac{d\Delta M}{dB}$.

Simultaneously measured magnetocurrents also exhibit dependency on the magnetic field strength and direction (Fig. 1). The directional asymmetry is even more pronounced

in the magnetocurrent curves obtained at relatively short times (Fig. S3). The area enclosed between the two magnetocurrent curves and the magnetic field at which the two curves cross one another is strongly time-dependent (Fig. S3). The asymmetry of the hysteresis loops and thus the dependence on magnetic field direction of both electrochemical current density and MOKE signal disappears at higher measurement times (Fig. S3). However, the equilibrium is only reached on a time-scale of several tens of minutes (Fig. 3), indicating that the magnetic-field dependence originates from non-equilibrium conditions induced by the application of the magnetic field. The MOKE enhancement factor changes with the same rate as the asymmetry of the magnetocurrent loops and the magnetic field at which the current loops intersect (Fig S3). Thus, the small changes of the MOKE signal and the magnetocurrent loops can be attributed to the same origin.

The change in the current density does not scale with the magnetic field strength (Fig. 1). As the magnetic field increases from 0 to 260 mT, current density does not continuously increase, but rather increases to a certain point (around 100 mT), after which a decrease is observed. This turning point coincides with the saturation of the MOKE hysteresis curves.

Discussion

The process induced by the presence of the magnetic field is slow relative to most electrochemical processes, reversible and affects simultaneously magnetic properties of the electrolyte and the overall current density (Fig. 1). The time-scale is in the order of diffusion processes facilitated by a magnetic
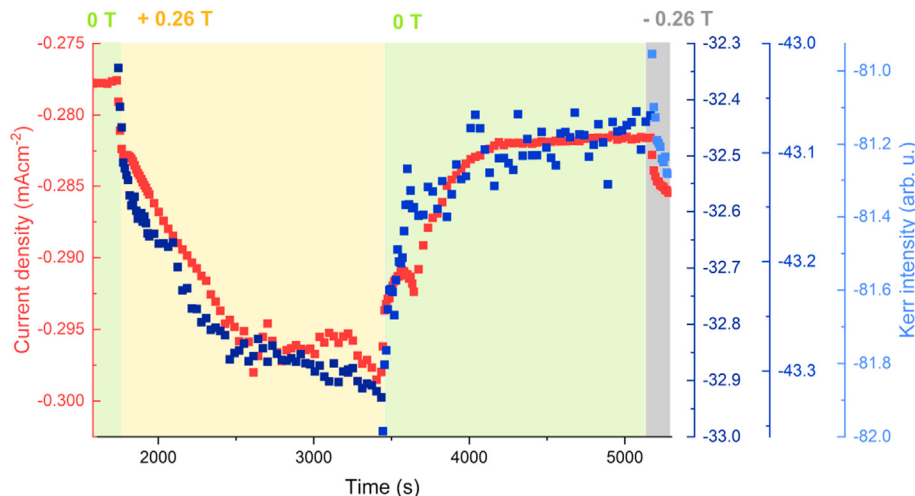
Fig. 3 – Magneto-optical Kerr intensity (blue) and current density (red) in cycled magnetic field: zero (green area), +0.26 T (yellow area) and −0.26 T (gray area). (For interpretation of the references to colour in this figure legend, the reader is referred to the Web version of this article.)

field gradient [28–30]. This so-called magneto-migration is a relatively small effect: concentration gradients of a few percent per cm develop on a timescale of hours in inhomogeneous magnetic field gradient of about T/cm applied to rare-earth ions [28–30]. The particle current density $J = j/(N_A ze)$ induced by chemical diffusion is enhanced by magnetic field gradient according to the thermodynamics of irreversible processes [31,32]:

$$J = -L \cdot \nabla \left(\mu_{chem} + \mu_{mag} \right) \tag{4}$$

where the chemical potential $\mu_{chem} \simeq RT = 2.5 \cdot 10^3 Jmol^{-1}$ and the magnetic energy is defined by:

$$\mu_{mag} = \frac{1}{2\mu_0} \cdot \chi B^2 \tag{5}$$

where $\chi = (1-c)\chi_{H_2O} - c\chi_{OH^-}$ is the difference in the magnetic susceptibility between H_2O and OH^- [33], μ_0 is the vacuum permeability, c the concentration of hydroxide ions and the tensor L contains the transport coefficients [31]. The overall magnetic energy contribution at maximum concentration difference c is $\simeq 10^{-5} Jmol^{-1}$ at $\chi_{max} \simeq (-13 + 11)10^{-12} m^3 \cdot mol^{-1}$, i.e. effectively negligible. However, where the reaction takes place, at the interface, the local concentration gradients of water and hydroxide ions can be large due the nanometer thickness of the EDL. The driving force induced by a constant magnetic field is then

$$J \propto \nabla(\chi B^2) \propto \chi B^2 \nabla c \tag{6}$$

With this, the impact of the magnetic energy in Eq. (4) relative to that of the overall diffusion loss, estimated by the ratio

$$\left(\frac{\Delta \mu_{mag}}{\Delta x_{EDL}} \right) \bigg/ \left(\frac{\Delta \mu_{chem}}{\Delta x_{chem}} \right) \simeq \left(\frac{10^{-5}}{10^{-8}} \right) \bigg/ \left(\frac{10^3}{10^{-1}} \right) = 10^{-1} \tag{7}$$

is markedly increased, and causes a local segregation of water and hydroxide ions with direct consequences on the electrochemical conversion in the order of a few %, as observed

experimentally. The effect was already observed for paramagnetic ions (nitrobenzene radicals) by Dunne et al. [15], but not for the diamagnetic aqueous systems. Our observation, which are smaller in magnitude, are in perfect agreement with these results, as $\Delta\chi_{dia} = -1/(10...1000)\Delta\chi_{para}$.

To corroborate this hypothesis, we performed experiments with various concentrations of KOH. Indeed, at 1 mM KOH concentrations there is no detectable effect, and with increasing pH, i.e. increasing number of ions, the effect becomes more pronounced (Fig. S4).

The effect is restricted to the hydrogen evolution, supporting the outlined hypothesis. Oxygen evolution is proportional to the number of ions, which are attracted by the electric field to the electrode (Eq. (2)). This is not the case in the HER (Eq. (1)) where the reactant is neutral water transported by diffusion. Its concentration has direct impact on the formation of hydroxide ions and thus on the electrochemical current density.

Dunne and Coey [16] studied the concept of magnetic forces and pressures as the origin of convection induced by magnetic field gradient. They emphasize the importance of the orthogonal component between the concentration and magnetic field gradients for facilitating convection. Our approximations omit the directional relation and only rationalize the magnitude of the effect, as defining the effect more precisely requires the exact knowledge of the magnetic field on the nanoscale [16,32] (refer to subsection C.1 for further details).

It has recently been reported that the maximum magnetization of the materials scales with the strength of the induced magnetocurrents [11]. Although the origin of the effect is not known, it was hypothesized that the changed spin-spin interactions during biradical recombination step of oxygen evolution reaction were the driving force, in line with the processes previously reported for other electrodes [12] and molecular systems [14,20]. In the given study direct spin-spin interactions can be neglected, as the interfacial metal is Pt. We

prove that the magnetic-field effect mainly influences the concentration of ions near the electrode-electrolyte interface, which explains quantitatively the dependence of the current on magnetic field, potential and time. At high current densities and fields, additional effects, e.g. bubbles, may become relevant (refer to subsection C.1 for further details). Our results are in line with the previously demonstrated influence of macroscopic magnetic array on the patterning during electrodeposition [16], which reports on the importance of the specific magnetic field curves and corresponding gradients.

Apart from electrolysis, the effect may be applicable in spintronics, as the accumulation of spins at ferromagnetic - paramagnetic metallic interfaces is based on similar dependencies [34]. Goboret et al. [32] point out applications in microbiology [35] and biomedicine, while further studies may contribute to the ongoing debate on the potential health ef-

Appendix A. Set-up for in situ magneto- and electro-optical Kerr effect analysis

The constructed magneto-optical Kerr effect set-up (Fig. A.4) for in situ probing of the electrochemical interfaces is adapted for electrode surfaces from previous publications. All components were purchased from *Thorlabs*, unless otherwise stated.
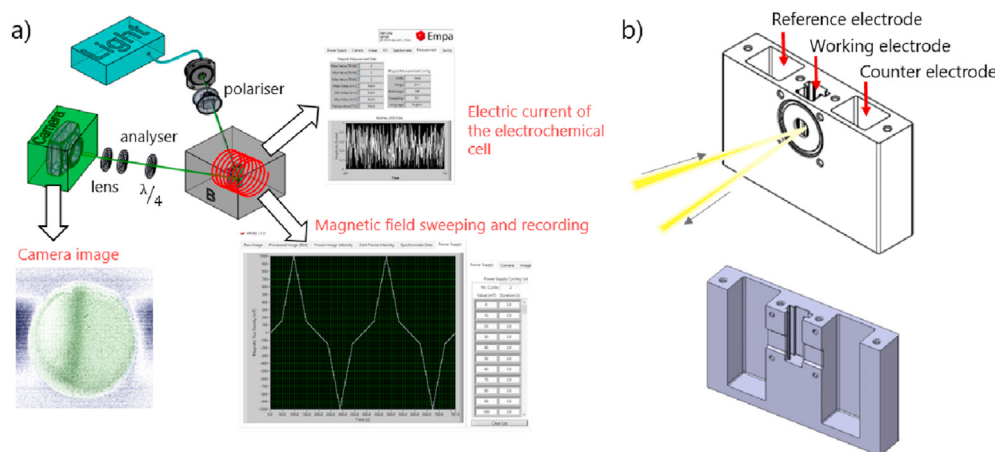

Figure A.4 – Magneto-optical Kerr effect set-up: a) Schematic representation of the set-up arrangement and main components; b) Sketch of the 3D printed electrochemical cell. The cross-section demonstrating interconnected electrode compartments is presented on the bottom.

fects as a result of the magnetic field exposure [36].

Conclusions

We report an enhancement of approximately 7% in the electrochemical hydrogen evolution on Pt electrodes exposed to moderate magnetic fields. The simultaneous in situ probing of magneto-optical properties and magnetocurrents provides evidence that the external magnetic fields affect the concentration gradient of hydroxide ions in the vicinity of the electrode surface established during hydrogen evolution. As water and hydroxide ions have different diamagnetic properties, this gradient is affected even by a constant magnetic field.

Declaration of competing interest

The authors declare that they have no known competing financial interests or personal relationships that could have appeared to influence the work reported in this paper.

Polar MOKE optical arrangement is selectively sensitive to out-of-plane magnetization (e.g. Co/Pt superlattice) and has orders of magnitude stronger signal than either longitudinal or transverse MOKE. Fully s-polarized probing light is achieved by passing a beam of a broadband light-emitting diode (MCWHF2) through a Glan-Thompson calcite polariser (GTH5M-A) (Fig. A.4). The light is reflected from a sample inserted into an electromagnet (max. 270 mT) equipped with a polarity switch and a magnetometer (*Wuntronic*, Koshava 5). Due to the birefringent properties of matter the light reflected from the magnetized sample surface is rotated by an angle, θ, so the reflected beam consists of a small p-polarized component (E_p) in addition to the dominant s-polarized one (E_s). The Kerr angle is defined by E_p/E_s and is directly proportional to the light intensity passing through the analyzer: the second polarizer that is set to near extinction (87°) relative to the initial polarizer.

Overall, the degree of rotation is detected through a combination of an analyzer (LPVISE100-A), plano convex lens (LA1433) and a complementary metal oxide semiconductor

(CMOS) camera (DCC1545 M), with the overall spatial resolution of the set-up of 55 μm.

The set-up is fitted with a 3D-printed polypropylene electrochemical cell (Fig. A.4) with three interconnected compartments: for working, counter and reference electrodes. The total volume of the cell is 25 ml. The working electrode is probed by light passing through the glass window and a layer of electrolyte. The applied potential and current flowing through the electrochemical cell is controlled and recorded with a potentiostat.

Probing depth of MOKE is defined by the attenuation length of visible light in metals that is on the order of 10 nm. Since MOKE is a reflection-based technique, the probing depth is in the range of 5 nm.

Appendix B. Electrode and electrolyte

The Co/Pt superlattice stack from substrate to top layer was grown by DC magnetron sputtering at around 2 μbar Ar atmosphere as follows: Al_2O_3 (0001)/Pt (10 nm)/[Co(0.4 nm)/Pt(0.7 nm)]$_5$/Pt(3 nm). The Pt (10 nm) layer acted as a seed layer and was grown at 400 °C. High temperature growth leads to epitaxial relation between the Pt seed layer and the substrate resulting in epitaxial Pt (111) layer. The subsequent layers [Co(0.4 nm)/Pt(0.7 nm)]$_5$/Pt(3 nm) were grown at room temperature after overnight cooling down. The sample shows 150 mT coercive field at 300 K measured by a vibrating-sample magnetometer. The surface area of the working electrode is 1 cm^2.

Platinum wire was used as a counter electrode (with a total surface area of 34 cm^2) and Hg/HgO as a reference electrode.

Potassium hydroxide pellets were purchased from Sigma-Aldrich and dissolved in MilliQ H_2O to 0.1 M concentration, unless stated otherwise. Iron impurities were removed according to the procedure outlined by Trotochaud et al. [37].

Appendix C. Estimation of MOKE enhancement factor

The MOKE enhancement factor may be calculated as described in Ref. [27]:

$$f_e^c = Abs\left(1 + \frac{4\pi i \tilde{n}_{CoPt} d}{\lambda} \frac{\tilde{n}_{EDL}^2 - \tilde{n}_0^2}{\tilde{n}_{CoPt}^2 - n_0^2}\right) \tag{C.1}$$

where λ is the incident wavelength, d the thickness of the EDL and $\tilde{n}_i$ is the complex index of refraction $\tilde{n}_i = n + ik$. The refractive index n of water and 0.1 M aqueous KOH is 1.33 and 1.37, respectively, and $k = 0$. $\tilde{n}_{CoPt} = 2.2 + i \cdot 4.2$. We assume a thickness of the EDL of around d = 2 nm.

Appendix C.1. Magneto-hydrodynamics

The electrolyte near to an electrochemically active electrode may be divided into three zones: the electrochemical double layer ($\delta_{EDL} \simeq 1$ nm), the diffusion layer ($nm < \delta_{diff} < 100$ μm, e.g. $\delta_{diff} = 15$ μm @ $j = 194$ mAcm^{-2} [38]) and the convection zone [38]. In principle, magnetic fields can affect all zones, i.e. the EDL [15], diffusion layer [28–30], and convection [15]. Convection is only affected by magnetic fields, if the concentration gradient and the field gradient have orthogonal components [16]. Bubbles are assigned to the convection zone, and their formation is influenced by magnetic fields [19,39]. The origin of magneto-hydrodynamic effect is a uniform magnetic field acting on a current via the Lorentz force [13]. In this paper, the electrolyte changes can be traced back to the first nm of the electrolyte adjacent to the electrode surface. The typical time constants found are indicative of diffusion processes [16]. Therefore, the magnetic field effects studied here can be traced back to their impact on the diffusion layer.

Appendix D. Supplementary data

Supplementary data to this article can be found online at https://doi.org/10.1016/j.ijhydene.2020.10.210.

REFERENCES

[1] Züttel A, Remhof A, Borgschulte A, Friedrichs O. Hydrogen: the future energy carrier. Phil Trans R Soc A 2010;368:3329.

[2] Borgschulte A. The hydrogen grand challenge. Front Energy Res 2016;4:11.

[3] Grim RG, Huang Z, Guarnieri MT, Ferrell JR, Tao L, Schaidle JA. Transforming the carbon economy: challenges and opportunities in the convergence of low-cost electricity and reductive CO_2 utilization. Energy Environ Sci 2020;13:472–94.

[4] Winter C-J. Hydrogen energy — abundant, efficient, clean: a debate over the energy-system-of-change. Int J Hydrogen Energy 2009;34:S1–52. https://doi.org/10.1016/j.ijhydene.2009.05.063. URL, http://www.sciencedirect.com/science/article/pii/S0360319909007691 [hydrogen Energy - Abundant, Efficient, Clean A Debate over the Energy-System-of-Change].

[5] Licht S, Wang B, Mukerji S, Soga T, Umeno M, Tributsch H. Over 18% solar energy conversion to generation of hydrogen fuel; theory and experiment for efficient solar water splitting. Int J Hydrogen Energy 2001;26:653–9. https://doi.org/10.1016/S0360-3199(00)00133-6. URL: http://www.sciencedirect.com/science/article/pii/S0360319900001336.

[6] Zeng K, Zhang D. Recent progress in alkaline water electrolysis for hydrogen production and applications, Progr. Energ. Combust Sci 2010;36:307–26.

[7] Marini S, Salvi P, Nelli P, Pesenti R, Villa M, Berrettoni M, Zangari G, Kiros Y. Transforming the carbon economy: challenges and opportunities in the convergence of low-cost electricity and reductive CO_2 utilization. Electrochim Acta 2012;82:384.

[8] Carmo M, Stolten D. Chapter 4 - energy storage using hydrogen produced from excess renewable electricity: power to hydrogen. In: de Miranda PEV, editor. Science and engineering of hydrogen-based energy technologies. Academic Press; 2019. p. 165–99.

[9] Barbir F, Gómez T. Efficiency and economics of proton exchange membrane (pem) fuel cells. Int J Hydrogen Energy 1997;22:1027–37. https://doi.org/10.1016/S0360-3199(96)00175-9. URL: http://www.sciencedirect.com/science/article/pii/S0360319996001759.

[10] LeRoy RL. Industrial water electrolysis: present and future. Int J Hydrogen Energy 1983;8:401–17.

[11] Garcés-Pineda F, Blasco-Ahicart M, Nieto-Castro D, et al. Direct magnetic enhancement of electrocatalytic water oxidation in alkaline media. Nat Energy 2019;4:519–25.

[12] Zhou W, Chen M, Guo M, Hong A, Yu T, Luo X, Yuan C, Lei W, Wang S. Magnetic enhancement for hydrogen evolution reaction on ferromagnetic MoS_2 catalyst. Nano Lett 2020;20:2923–30.

[13] Lin M-Y, Hourng L-W, Kuo C-W. The effect of magnetic force on hydrogen production efficiency in water electrolysis. Int J Hydrogen Energy 2012;37:1311–20. https://doi.org/10.1016/j.ijhydene.2011.10.024. URL: http://www.sciencedirect.com/science/article/pii/S0360319911023500. 10th International Conference on Clean Energy 2010.

[14] Steiner UE, Ulrich T. Magnetic field effects in chemical kinetics and related phenomena. Chem Rev 1989;89:51–147.

[15] Dunne P, Coey JMD. Influence of a magnetic field on the electrochemical double layer. J Phys Chem C 2019;123:24181–92.

[16] Dunne P, Coey JMD. Patterning metallic electrodeposits with magnet arrays. Phys Rev B 2012;85:224411.

[17] Mohanta S, Fahidy T. Mass transfer in a magnetoelectrolytic flow cell. Electrochim Acta 1974;19:835–40.

[18] Monzon LM, Coey J. Magnetic fields in electrochemistry: the lorentz force. a mini-review. Electrochem Commun 2014;42:38–41.

[19] Koza JA, Mühlenhoff S, Żabiński P, Nikrityuk PA, Eckert K, Uhlemann M, Gebert A, Weier T, Schultz L, Odenbach S. Hydrogen evolution under the influence of a magnetic field. Electrochim Acta 2011;56:2665–75.

[20] Mtangi W, Tassinari F, Vankayala K, Vargas Jentzsch A, Adelizzi B, Palmans ARA, Fontanesi C, Meijer EW, Naaman R. Control of electrons' spin eliminates hydrogen peroxide formation during water splitting. J Am Chem Soc 2017;139:2794–8.

[21] Aaboubi O. Hydrogen evolution activity of ni–mo coating electrodeposited under magnetic field control. Int J Hydrogen Energy 2011;36:4702–9.

[22] Weisheit M, Fähler S, Marty A, Souche Y, Poinsignon C, Givord D. Electric field-induced modification of magnetism in thin-film. ferromagnets 2007;315:349–51.

[23] Zeper WB, Greidanus FJAM, Carcia PF, Fincher CR. Perpendicular magnetic anisotropy and magneto-optical Kerr effect of vapor deposited Co/Pt-layered structures. J Appl Phys 1989;65:4971.

[24] Bertero G, Sinclair R. Structure-property correlations in Pt/Co multilayers for magneto-optic recording. J of Magn Magn Mater 1994;134:173–84.

[25] Lee TY, Chan Won Y, Su Son D, Ho Lim S, Lee S-R. Effects of co layer thickness and annealing temperature on the magnetic properties of inverted [pt/co] multilayers. J Appl Phys 2013;114:173909.

[26] Tokunaga E, Nosaka Y, Hirabayashi M, Kobayashi T. Pockels effect of water in the electric double layer at the interface between water and transparent electrode. Surf Sci 2007;601:735–41.

[27] You C-Y, Shin S-C. First-order approximations of the general magneto-optical kerr effects for an optically thin capping layer. Thin Solid Films 2005;493:226–9.

[28] Franczak A, Binnemans K, Fransaer J. Magnetomigration of rare-earth ions in inhomogeneous magnetic fields. Phys Chem Chem Phys 2016;18:27342.

[29] Pulko B, Yang X, Lei Z, Odenbach S, Eckert K. Magnetic separation of Dy(III) ions from homogeneous aqueous solutions. Appl Phys Lett 2014;105:232407.

[30] Fujiwara M, Chie K, Sawai J, Shimizu D, Tanimoto Y. On the movement of paramagnetic ions in an inhomogeneous magnetic field. J Phys Chem B 2004;108:3531–4.

[31] Onsager L. Reciprocal relations in irreversible processes. I. Phys Rev 1931;37:405–26.

[32] Gorobets OY, Gorobets YI, Rospotniuk VP. Magnetophoretic potential at the movement of cluster products of electrochemical reactions in an inhomogeneous magnetic field. J Appl Phys 2015;118:073902.

[33] Rumble John R, editor. CRC handbook of chemistry and physics. 100 ed. CRC press, Taylor & Francis Group; 2019.

[34] Sears MR, Saslow WM. Spin accumulation at ferromagnet/nonmagnetic material interfaces. Phys Rev B 2012;85:014404.

[35] Blakemore R. Magnetotactic bacteria. Science 1975;190:377–9. https://doi.org/10.1126/science.170679.

[36] Feychting M. Health effects of static magnetic fields—a review of the epidemiological evidence. Prog Biophys Mol Biol 2005;87:241–6.

[37] Trotochaud L, Young SL, Ranney JK, Boettcher SW. Nickel-Iron oxyhydroxide oxygen-evolution electrocatalysts: the role of intentional and incidental iron incorporation. J Am Chem Soc 2014;136:6744–53. https://doi.org/10.1021/ja502379c.

[38] Li S. Chapter 13 - introduction to electrochemical reaction engineering. In: Li S, editor. Reaction engineering. Boston: Butterworth-Heinemann; 2017. p. 599–651.

[39] Njoka F, Mori S, Ookawara S, Ahmed M. Effects of photo-generated gas bubbles on the performance of tandem photoelectrochemical reactors for hydrogen production. Int J Hydrogen Energy 2019;44:10286–300. https://doi.org/10.1016/j.ijhydene.2019.02.194. URL: http://www.sciencedirect.com/science/article/pii/S0360319919308523.